CHAPTER IV
RESULTS AND DISCUSSION

4.1 Characterization Results

The unimpregnated and impregnated adsorbents were characterized. GC-FID was used to measure the degree of PZ loading. Scanning Electron Microscope (SEM) was employed to study the morphology of the adsorbents. Surface area analysis was used to determine surface area, pore size and pore volume, and the thermal stability was investigated by thermo gravimetric analysis (TGA).

4.1.1 Analysis of Piperazine Loading (wt %)

To investigate the amount of PZ on the impregnated AC and SG, GC-FID was used to measure the PZ loading. A calibration curve that obtained from GC-FID shown in Figure 4.1 was done to determine the concentration of an unknown sample in the adsorbent by comparing with PZ standards of known concentration. The plots were then fitted into a straight line, using linear regression which can be described by the linear equation, $y = 16.203x + 2.2933$, where y is the area, 16.203 is sensitivity and 2.2933 is the interception and x is the analyzed concentration of unknown samples. The PZ standard of known concentration showed the coefficient of determination, $R^2 = 0.9994$. The result showed the average of 3.45 wt % and 8.33 wt % of PZ loaded on the AC and SG, respectively. It is interesting to note that the different types of adsorbent showed the different PZ loading because of the different natural pore structures. To understand the types of adsorbent more clearly, scanning electron microscope (SEM) was applied to observe the morphology of adsorbents.

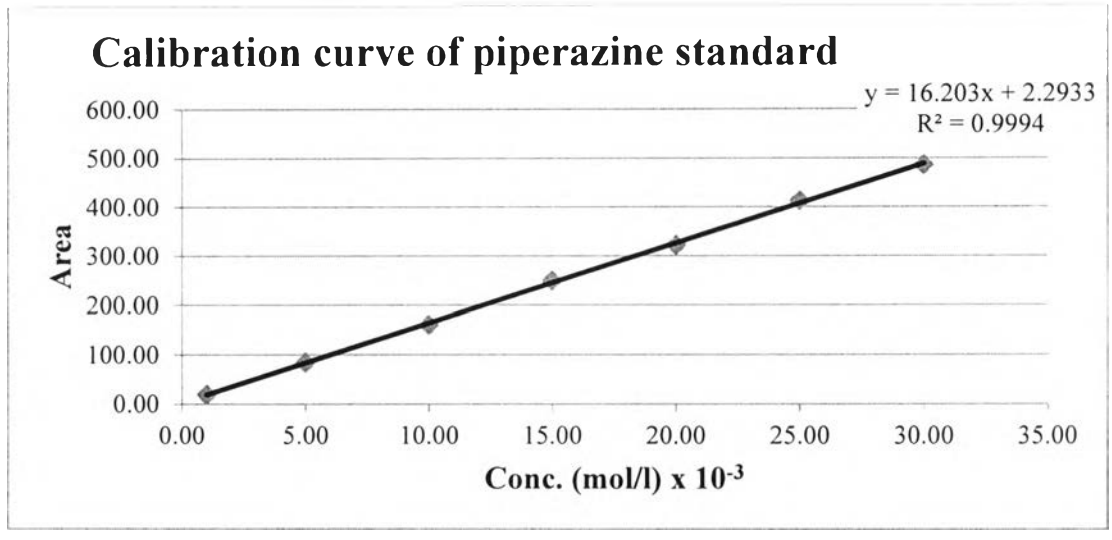

Figure 4.1 Calibration curve of piperazine standard of known concentration.

4.1.2 Scanning Electron Microscope (SEM) & Surface Area Analysis

Scanning electron microscope (SEM) with a magnification of 9000 times was used to distinguish the morphology of adsorbents between the unimpregnated and impregnated adsorbents. Figure 4.2 demonstrates the surface morphology of (a) the unimpregnated AC, (b) impregnated AC (20-40 mesh size), (c) unimpregnated SG, and (d) impregnated SG. The morphology of the unimpregnated adsorbents of Figure 4.2(a) and (c) indicates the differences of surface and pores of AC and SG. Pure AC shows rougher surface and more pores than pure SG. By the comparison between unimpregnated and impregnated adsorbents, Figure 4.2(b) shows the impregnated AC with some amount of PZ, while for impregnated SG, there is a slight difference in the surface and pore size. In SEM results, it was able to observe only the macropore (pore size diameter > 50 nm) and the changing in smaller pore structure cannot be found. To understand the surface morphology more clearly, surface area analysis was applied in order to distinguish the changes of unimpregnated and impregnated adsorbents surface area and pore volume.

PCL XL Error
Subsystem: I/O
Error: InputReadError
Operator: ReadImage
Position: 23188

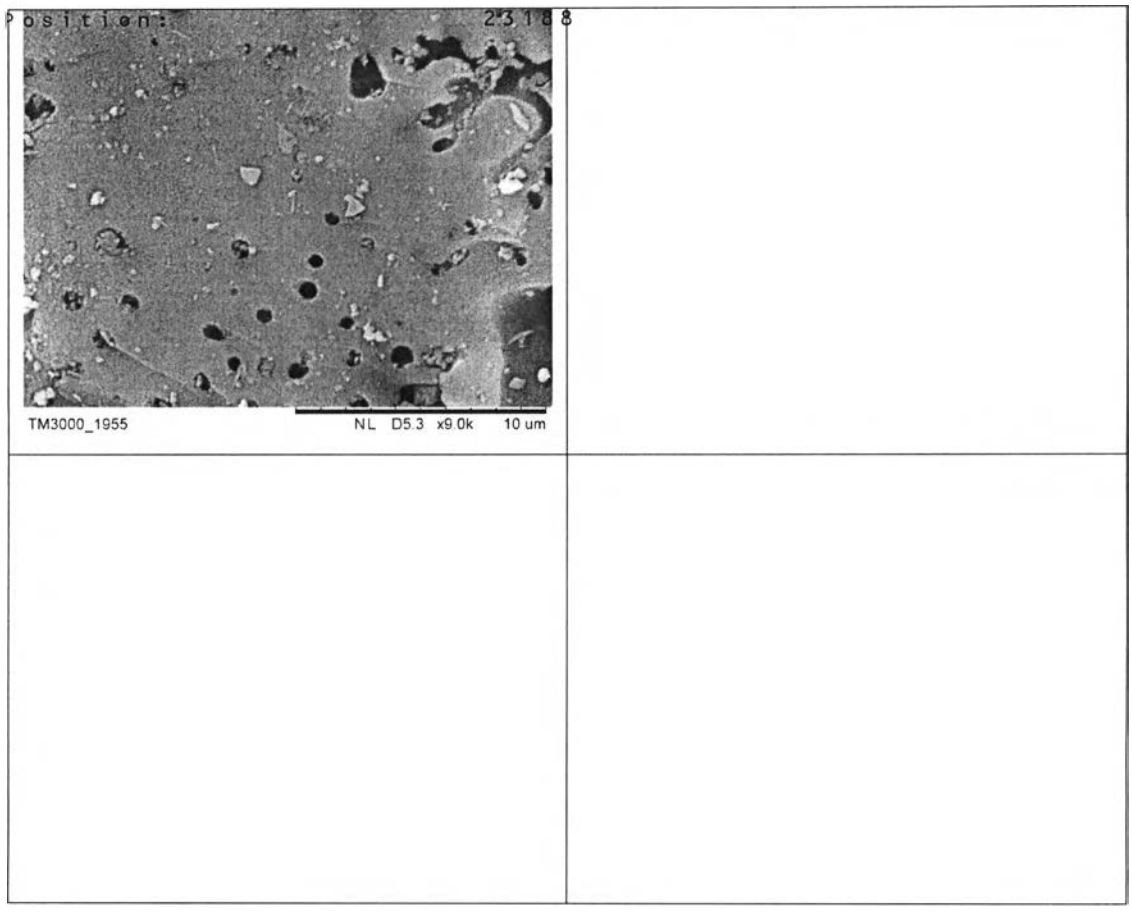

Figure 4.2 SEM micrographs of (a) unimpregnated AC, (b) impregnated AC, (c) unimpregnated SG, (d) impregnated SG.

The surface area analysis of AC and SG samples was investigated in order to precisely determine the effect of adsorbent types by using a nitrogen adsorption at 77 K. According to the International Union of Pure and Applied Chemistry (IUPAC), pores on AC and SG are classified by their sizes into three groups: macropores having an average diameter of greater than 50 nm, mesopores with a diameter of 2–50 nm, and micropores having an average diameter of less than 2 nm.

Sakpal *et al.* (2012) observed that the CO_2 adsorption capacity of the SG particles increase with smaller particle size. The SG particle sizes are varied from 60-120, 100-200, and 230-400 mesh. The 230-400 mesh exhibited the largest adsorption capacity at 275 K at 142 mg of CO_2/g of adsorbent because of the highest

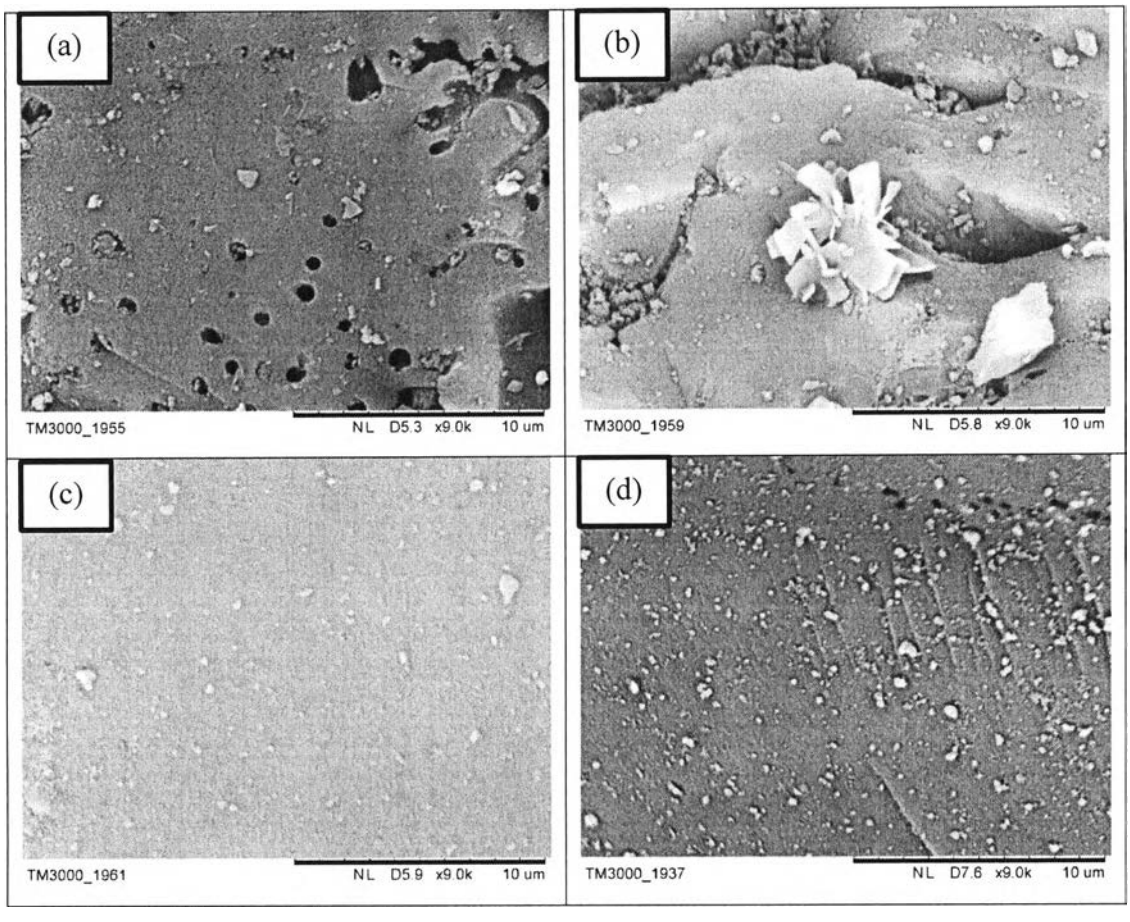

Figure 4.2 SEM micrographs of (a) unimpregnated AC, (b) impregnated AC, (c) unimpregnated SG, (d) impregnated SG.

The surface area analysis of AC and SG samples was investigated in order to precisely determine the effect of adsorbent types by using a nitrogen adsorption at 77 K. According to the International Union of Pure and Applied Chemistry (IUPAC), pores on AC and SG are classified by their sizes into three groups: macropores having an average diameter of greater than 50 nm, mesopores with a diameter of 2–50 nm, and micropores having an average diameter of less than 2 nm.

Sakpal *et al.* (2012) observed that the CO_2 adsorption capacity of the SG particles increase with smaller particle size. The SG particle sizes are varied from 60-120, 100-200, and 230-400 mesh. The 230-400 mesh exhibited the largest adsorption capacity at 275 K at 142 mg of CO_2/g of adsorbent because of the highest

surface area. For AC particles, typically AC particle sizes between 0.4 and 2.5 mm (8-40 mesh) are used in CO_2 fixed bed adsorption. This size range results from a practical compromise between limiting the pressure drop and providing adequate surface area. Table 4.1 shows the surface area and pore volume of the unimpregnated and impregnated AC and SG. Surface area usually given as weight specific surface area, S_{BET}, was calculated using the BET equation. From Table 4.1, the total specific surface area of unimpregnated AC was higher than the value of unimpregnated SG due to the difference pore structures of AC and SG that AC contains micropores resulting in higher total specific surface area as compared to SG having no micropores. So, the surface area analysis indicates that the AC contains both of micropores and mesopores structure on their surface and the SG is only mesopores structure. However, the macropore can be neglected because of small amount of macropore (Bansal and Goyal, 2005).

Table 4.1 Surface area analysis of unimpregnated and impregnated AC and SG

Samples	S_{BET}[a] (m^2/g)	V_{total}[b] (cm^3/g)×10^{-1}	V_{micro}[c] (cm^3/g)×10^{-1}	V_{meso}[d] (cm^3/g)×10^{-1}	D_p[e] (Å)
unimpregnated AC	925.4	5.12	4.39	0.73	22.1
3.45 wt % PZ-AC	845.3	4.72	3.99	0.73	22.3
unimpregnated SG	557.3	7.92	-	7.92	56.9
8.33 wt % PZ-SG	478.7	6.75	-	6.75	56.4

[a]BET surface area. [b]Total pore volume and [c]Micropore volume calculated by t-Plot method. [d]Mesopore volume calculated by subtracting the volume of V_{micro} from V_{total}
[e]Average pore diameter.

The comparison between the surface area of unimpregnated AC and SG was evaluated by using BET method and it can be found that the surface area of the unimpregnated AC was 925.4 m^2/g. By using t-Plot method, the micropore volume of AC was accounted for the largest portion (86 %) of the total pore volume and the remaining pore volume which was the difference between the total and the micropore volumes was the combination volumes of the mesopore and the

macropore. If the macropore volume could be neglected, the mesopore volume of AC could be estimated around 14 %. For unimpregnated SG, the BET surface area was 557.3 m^2/g and total pore volume by the t-Plot method was 0.792 cm^3/g which was accounted for the mesopore volume. When impregnated with PZ, the surface area and the pore volume of the impregnated AC and SG were decrease. The decrease in the surface area is due to the loading of PZ. The increase of PZ in AC resulted in the decrease in total pore and micropore volumes. If the macropore of AC was neglected, the mesopore volume of AC would be determined from the difference between the total pore and micropore volumes. From the results, the mesopore volume of the unimpregnated and impregnated AC still unchanged (0.073 cm^3/g). It could indicate that the decrease in pore volume of AC mainly came from the micropore. It can be seen that the PZ loading is probably partially filling and/or blocking the micropore but does not see the change in the mesopore. For impregnated SG, there was a decrease in the surface area and the total pore volume because of the PZ loading. PZ loading in AC and SG were 3.45 % and 8.33 %, corresponding to the decrease of surface area of 8.7% and 14.1 %, and the total pore volume of 7.8 % and 14.8 %, respectively. AC has even higher surface area than SG, but lacks of PZ loading due to micropore blockage limitation.

Table 4.2 Summary of surface area analysis of unimpregnated and impregnated adsorbent

Adsorbent	Unimpregnated	impregnated	%change
Total surface area (m^2/g)			
• AC (20-40 mesh)	925.4	845.3	8.7
• SG (230-400 mesh)	557.3	478.7	14.1
Total pore volume (cm^3/g)$\times 10^{-1}$			
• AC (20-40 mesh)	5.12	4.72	7.8
• SG (230-400 mesh)	7.92	6.75	14.8

4.1.3 Thermogravimetric Analysis (TGA)

The thermal stability of adsorbents was investigated by thermogravimetric analysis to measure the amount of mass loss via a function of increasing temperature. The TG profiles of PZ, unimpregnated and impregnated adsorbents are presented in Figure 4.3 to Figure 4.5. The results showed that the decomposition temperature of PZ was 78.99 °C. To evaluate the stability of the impregnated adsorbents, pure AC, pure SG, 3.45 wt % PZ loaded on AC, and 8.33 wt % PZ loaded on SG were also determined as shown in Figure 4.4 to Figure 4.5. The pure AC and pure SG thermal stability results showed the slightly decrease of weight loss at 80 °C to 100 °C. At this range of temperature, the weight loss could be due to the removal of moisture. For the impregnated AC and the impregnated SG, the step of weight loss is the results from the removal of moisture and a decomposition of PZ. The impregnated AC and that of SG were decomposed at higher temperature of 80.35 °C and 81.02 °C, respectively. The complete decomposition of impregnated of AC and SG was around at 134-140 °C. These results were shift from the boiling point of PZ at 145 °C that could be due to the ramping rate of 10 °C/min. To apply the impregnated adsorbent used, the temperature of CO_2 adsorption and regeneration process should not above 80 °C.

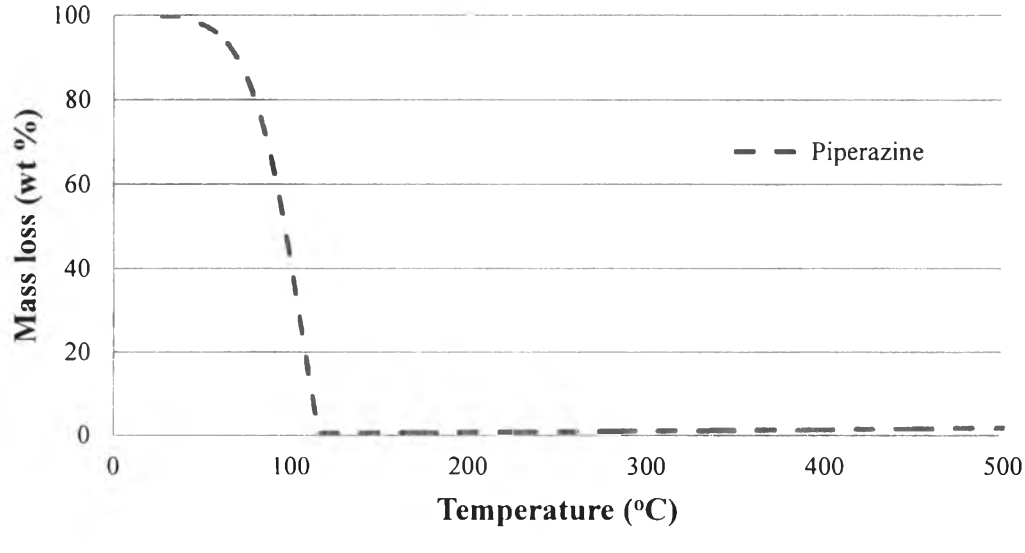

Figure 4.3 Thermal stability of PZ at room temperature to 500 °C.

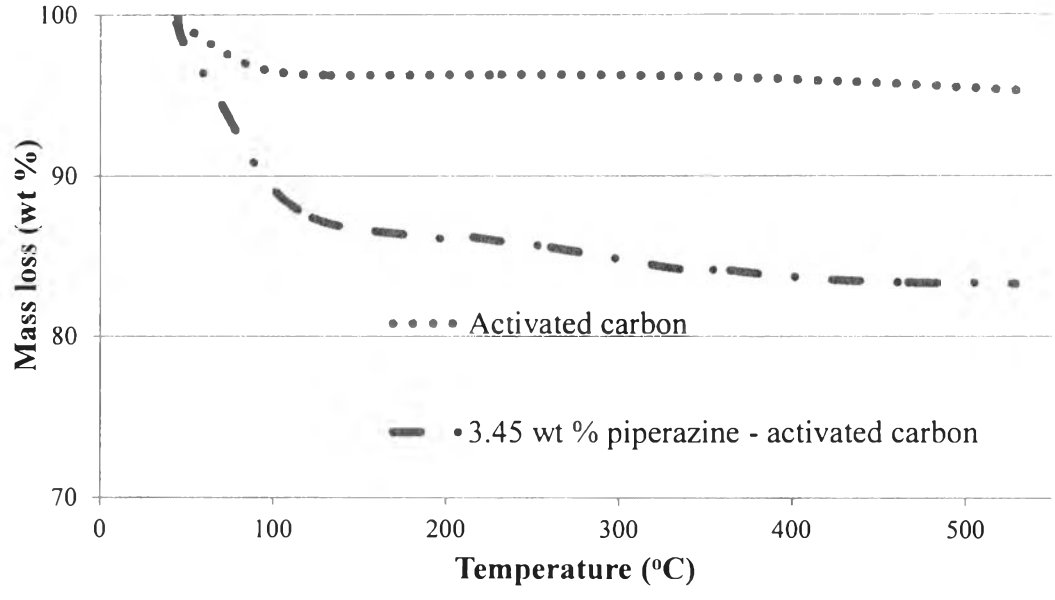

Figure 4.4 Thermal stability of acitvated carbon and 3.45 wt % PZ - AC at room temperature to 500 °C.

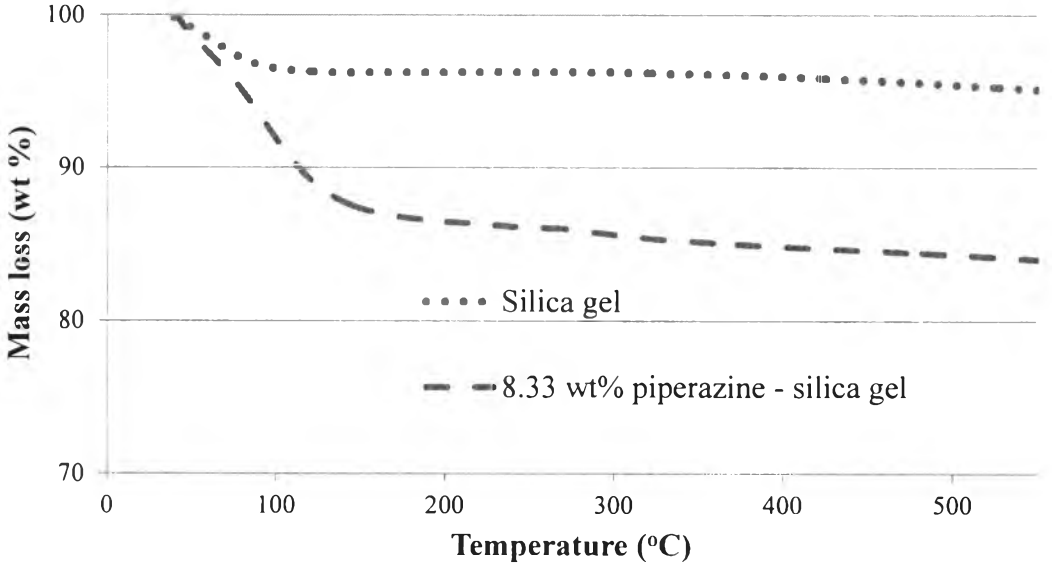

Figure 4.5 Thermal stability of SG and 8.33 wt % PZ - SG at room temperature to 500 °C.

4.2 Effects of Adsorption Pressure

Figure 4.6 and Figure 4.7 illustrate the breakthrough curves of pure AC and pure SG with different pressure at room temperature. For pure AC, the micropore volume was estimated around 86 % of the total pore volume and the rest is mesopore volume. For pure SG, the mesopore volume was accounted for 100 %. If the CO_2 adsorption capacity was accounted from the CO_2 molecules adsorbed by the surface and pore sites of adsorbent, the effect of pore sites in CO_2 adsorption capacity could be estimated to show the adsorption capacity per unit surface area of pure AC and pure SG.

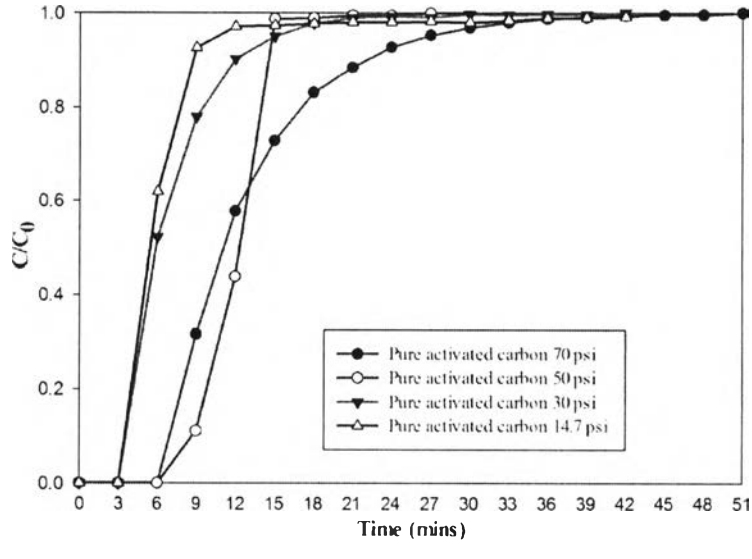

Figure 4.6 Breakthrough curves of pure AC at atmospheric pressure (14.7 psi), 30 psi, 50 psi, and 70 psi.

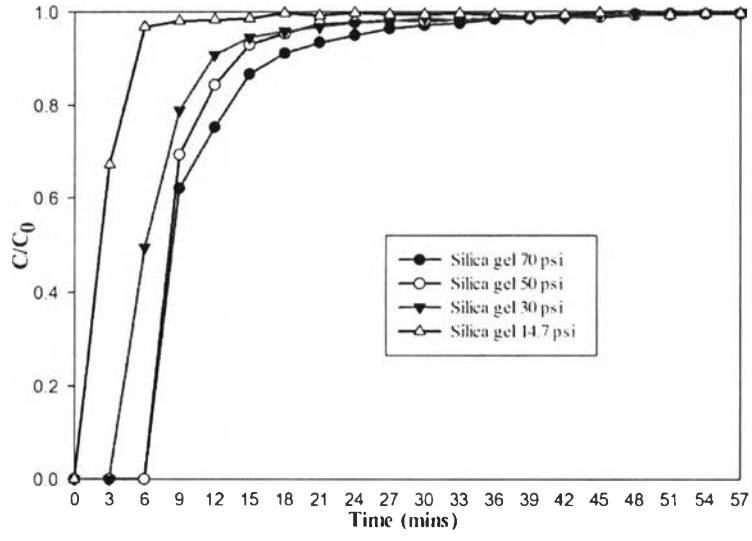

Figure 4.7 Breakthrough curves of pure SG at atmospheric pressure (14.7 psi), 30 psi, 50 psi, and 70 psi.

The increase of pressure leads to increase of CO_2 adsorption capacity which were 0.5943, 1.3551, 3.7368, and 5.7193 mmol/g for pure AC and 0.2462, 1.3174, 2.8984, and 4.7579 mmol/g for pure SG, at 14.7 psi, 30 psi, 50 psi, and 70 psi, respectively. In order to compare the CO_2 adsorption capacity, these results could be normalized to the CO_2 adsorption capacity (mmol/g) per surface area (m^2/g) as shown in Table 4.3.

Table 4.3 Normalized CO_2 adsorption capacity of pure adsorbent ($\mu mol/m^2 \cdot g$)

Condition	CO_2 adsorption capacity ($\mu mol/m^2 \cdot g$)	
Pressure (psi)	Pure AC (surface area 925.4 m^2/g)	Pure SG (surface area 557.3 m^2/g)
14.7	0.6422	0.4418
30	1.4643	2.3639
50	4.0380	5.2008
70	6.1804	8.5374

Basically, the process of CO_2 adsorption that takes place on a solid surface involves adsorption processes between the adsorbent and the CO_2 molecules. Adsorption in mesopores of SG could mainly dominate by multimolecular layer adsorption at the higher pressure. The multilayer adsorption is the process that the monomolecular adsorption will take place until the surface of the adsorbent becomes covered by a single layer of CO_2 molecules. When the first layer of CO_2 is complete, the formation of second and subsequent layers resulting in multilayer adsorption from CO_2 interact to the adsorbent, whereas the adsorption in micropores of AC could dominate by the strong interaction between CO_2 molecules and pore walls. Accordingly, the adsorption inside micropores could occur via the micropore filling at the atmospheric pressure. From Table 4.3, the normalized CO_2 adsorption capacity of pure AC was 0.6422 $\mu mol/m^2 \cdot g$ shows the higher value than the normalized capacity of pure SG (0.4418 $\mu mol/m^2 \cdot g$) at pressure 14.7 psi due to the difference of pores. The CO_2 adsorption capacity of pure SG could totally come from the mesopore, while for the pure AC, the CO_2 adsorption capacity from micropore (86 %) and mesopore (14 %). It might suppose that the larger portion of micropores in the AC could occur the micropore filling that could dominate the multilayer adsorption of mesopore SG at the atmospheric pressure. At the elevating pressure, both of pure AC and SG exhibited the increase of CO_2 adsorption capacity. The adsorption force was physisorption based on Van Der Waal force interacting between the exterior and pore interior surface of adsorbent and CO_2 molecules and the attractive force increase with increase in the adsorption pressure corresponding to the higher CO_2 adsorption capacity. For comparison between pure AC and pure SG at elevate pressure, the results show the contrast of the normalized CO_2 adsorption capacity of 14.7 psi. The normalized CO_2 adsorption capacity of pure AC shows the lower adsorption capacity than the pure SG at the same pressure condition. The mesopore of SG show dominate physisorption of the multilayer adsorption while for the micropore in AC, have the limitation of pore filling occuring at the higher pressure.

Figure 4.8 showed the example of comparison of the breakthrough curves at pressure 30 psi of (a) the unimpregnated and impregnated AC, and (b) the unimpregnated and impregnated SG. The adsorption capacities of unimpregnated and

impregnated adsorbents at 30 psi were 1.3551 and 2.2425 mmol/g for AC and 1.3174 and 2.3476 mmol/g for SG. The results showed that the impregnated adsorbent had the higher CO_2 adsorption capacity than the unimpregnated adsorbent. The results indicate that PZ enhances the adsorption of the unimpregnated adsorbent, probably, due to the chemical interaction between PZ active sites and CO_2 molecules.

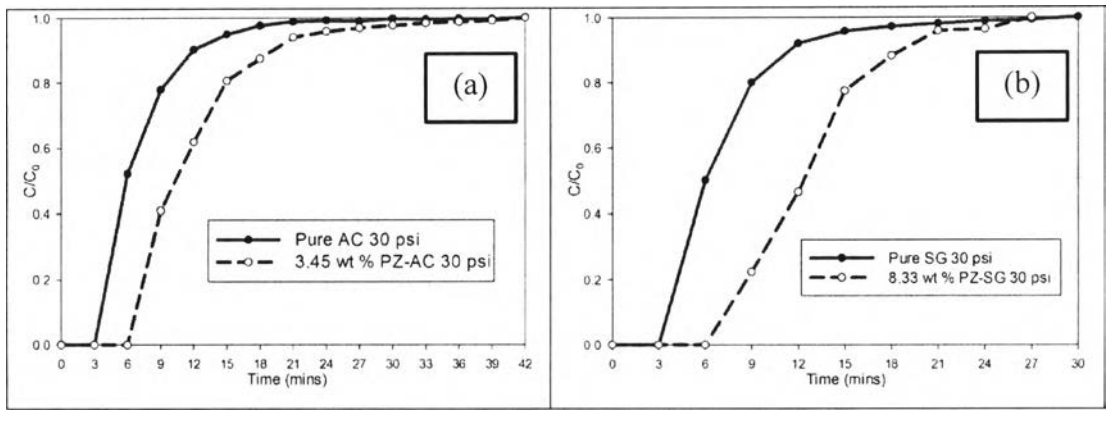

Figure 4.8 Breakthrough curves of (a) the unimpregnated and impregnated AC, and (b) the unimpregnated and impregnated SG at pressure 30 psi.

Figure 4.9 and Figure 4.10 illustrate the breakthrough curves of the impregnated AC and impregnated SG at different pressure and room temperature. From the breakthrough curve, the elevation of adsorption pressure took longer time to reach the saturation because the attractive force between the surface of the adsorbent and the CO_2 molecules is increase. Then, the results exhibited the increase of CO_2 adsorption capacity with the increase in pressure. The adsorption capacities of the impregnated adsorbents at 14.7 psi, 30 psi, 50 psi, and 70 psi were 0.6838, 2.2425, 4.1822, and 6.7199 mmol/g for 3.45 wt % PZ - AC and 0.6975, 2.3476, 4.4368, and 7.7340 mmol/g for 8.33 wt % PZ - SG, respectively. In order to compare the adsorption capacity of the unimpregnated and impregnated adsorbent, these results could be normalized to the CO_2 adsorption capacity (mmol/g) per surface area (m^2/g) as shown in Table 4.4.

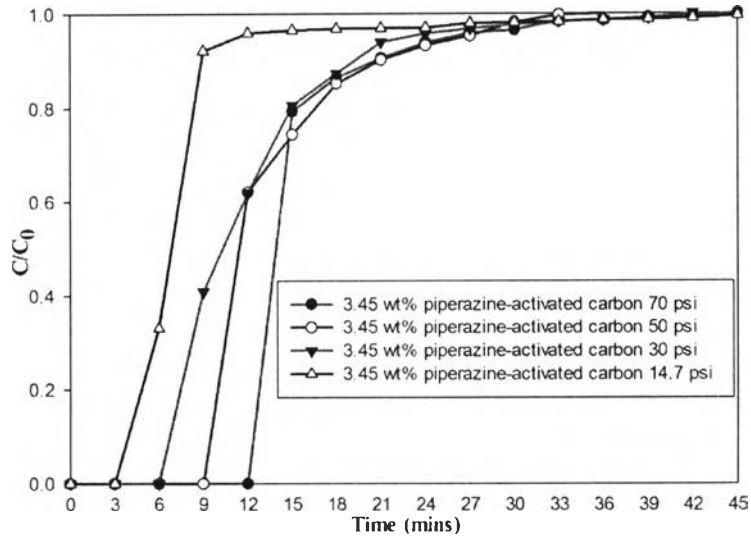

Figure 4.9 Breakthrough curves of impregnated AC at 14.7 psi, 30 psi, 50 psi, and 70 psi.

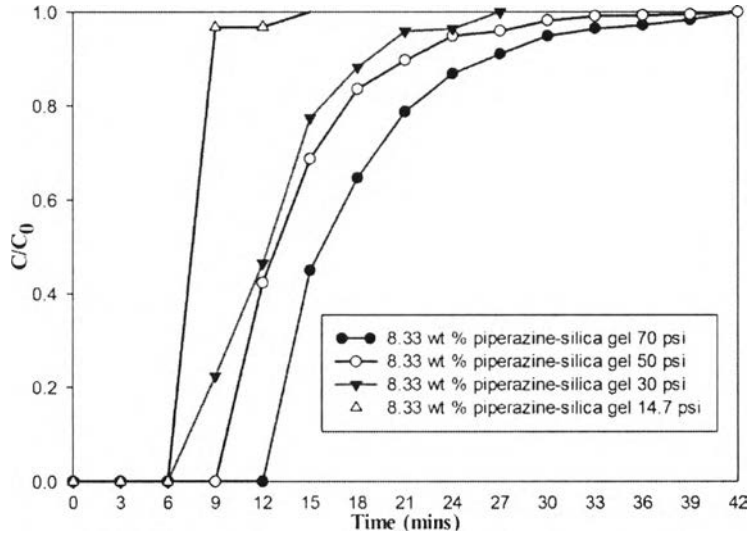

Figure 4.10 Breakthrough curves of impregnated SG at 14.7 psi, 30 psi, 50 psi, and 70 psi.

Table 4.4 Normalized CO_2 adsorption capacity between pure and impregnated adsorbent ($\mu mol/m^2 \cdot g$)

Condition	CO_2 adsorption capacity ($\mu mol/m^2 \cdot g$)			
Pressure (psi)	Pure AC (surface area 925.4 m^2/g)	3.45 wt % PZ-AC (surface area 845.3 m^2/g)	Pure SG (surface area 557.3 m^2/g)	8.33 wt % PZ-SG (surface area 478.7 m^2/g)
14.7	0.6422	0.8089	0.4418	1.4571
30	1.4643	2.6529	2.3639	4.9041
50	4.0380	4.9476	5.2008	9.2684
70	6.1804	7.9497	8.5374	16.1563

The comparison between the unimpregnated and impregnated AC at pressure 14.7 psi, the impregnated AC shows the normalized CO_2 adsorption capacity of 0.8089 $\mu mol/m^2$ which higher than the unimpregnated AC (0.6422 $\mu mol/m^2$) due to the enhancement of PZ. Corresponding to the elevating pressure, the impregnated AC shows the higher normalized CO_2 adsorption capacity. The results could come from the compatible between the physical and chemical adsorption on the impregnated AC that dominate the only physisorption on the unimpregnated AC. The increasing pressure increases the attractive force between adsorbent and CO_2 molecules. Then, the elevating pressure shows the higher adsorption capacity. For the impregnated SG, the results show the higher normalized CO_2 adsorption capacity than the unimpregnated SG at the same pressure condition. The results indicate that PZ contributes adsorption which enhances the physisorption of unimpregnated SG. The normalized CO_2 adsorption capacity of the impregnated SG demonstrates the higher value than the impregnated AC. The results could come from the enhancement of PZ that the impregnated SG can load the more amount of PZ with 8.33 wt %. Due to AC has the limitation of PZ loading of 3.45 wt % which occur the pore blocking in the micropore. To understand more clearly, the comparison of CO_2 adsorption capacity between unimpregnated and impregnated adsorbent is also

shown in Figure 4.11. The different pore sizes could be expected to exhibit different adsorption capacity during adsorption as pressure increases. The micropores of AC will experience physisorption of the pore-filling occurs at the atmospheric pressure (14.7 psi). At the elevation pressure, the impregnated AC shows the higher adsorption capacity because the enhancement of PZ could occur between nitrogen groups of PZ interact with CO_2 molecules. While for the mesopores of SG, the CO_2 adsorption could formed the single layer adsorption at the atmospheric pressure and multilayer adsorption at the higher pressure, but the impregnated SG still show the higher CO_2 adsorption capacity due to the enhancement of PZ.

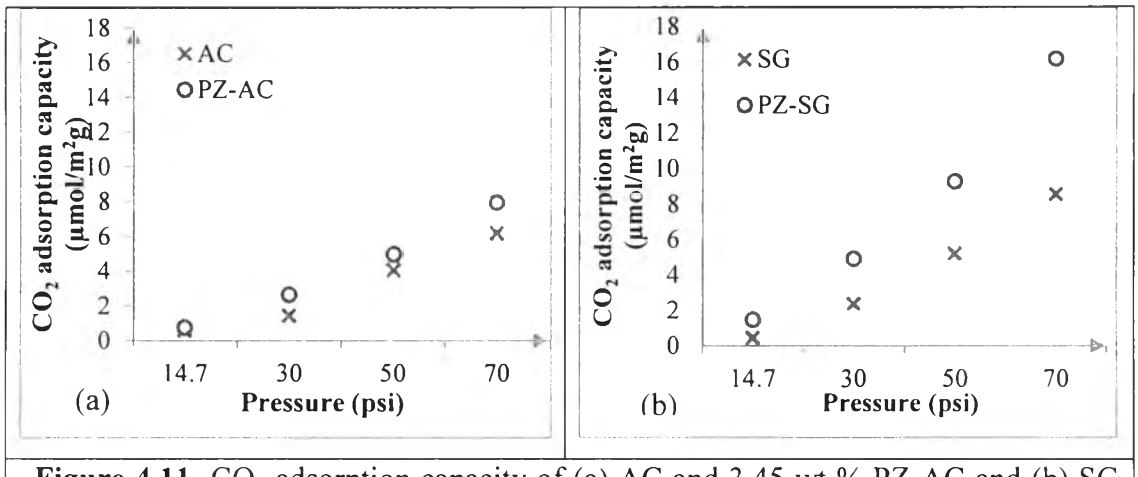

Figure 4.11 CO_2 adsorption capacity of (a) AC and 3.45 wt % PZ-AC and (b) SG and 8.33 wt % PZ-SG.

4.3 Regeneration

The regeneration stability of CO_2 adsorbents after many adsorption-regeneration cycles is important for practical application. Thus, the CO_2 adsorption-regeneration cycles were tested on the impregnated AC and SG. As shown in Figure 4.12 to Figure 4.19, the breakthrough curves of the regeneration were not exactly regain their original adsorption capacity during three consecutive test cycles. The regeneration was run after the adsorption cycle and the normalized CO_2 adsorption capacity of impregnated adsorbents was calculated as shown in Table 4.5 and Table 4.6 and summarized in Figure 4.20.

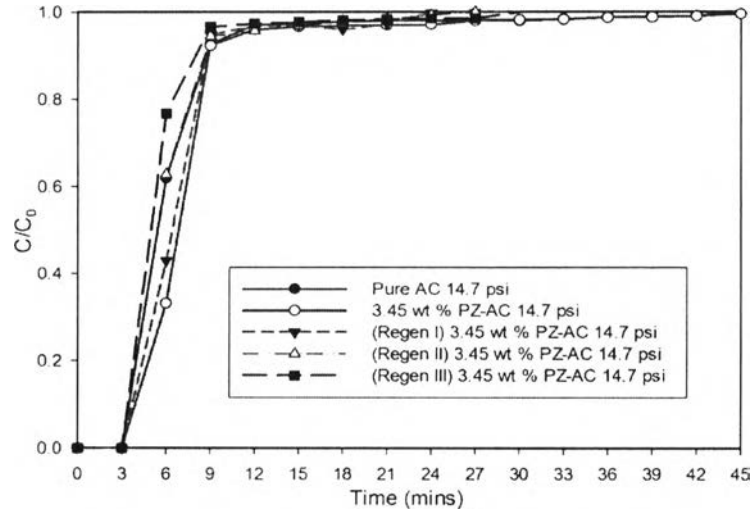

Figure 4.12 Breakthrough curves of PZ - AC adsorption at 14.7 psi, and regeneration cycle I, cycle II, cycle III at room temperature.

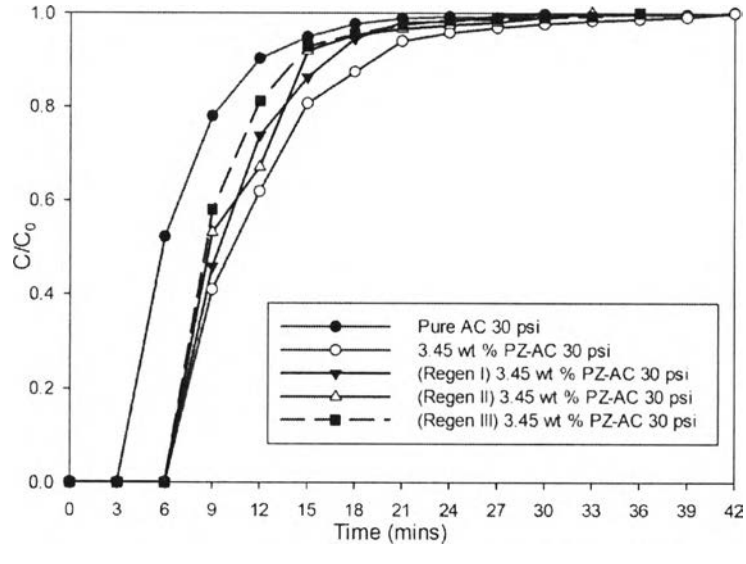

Figure 4.13 Breakthrough curves of PZ - AC adsorption at 30 psi, and regeneration cycle I, cycle II, cycle III at room temperature.

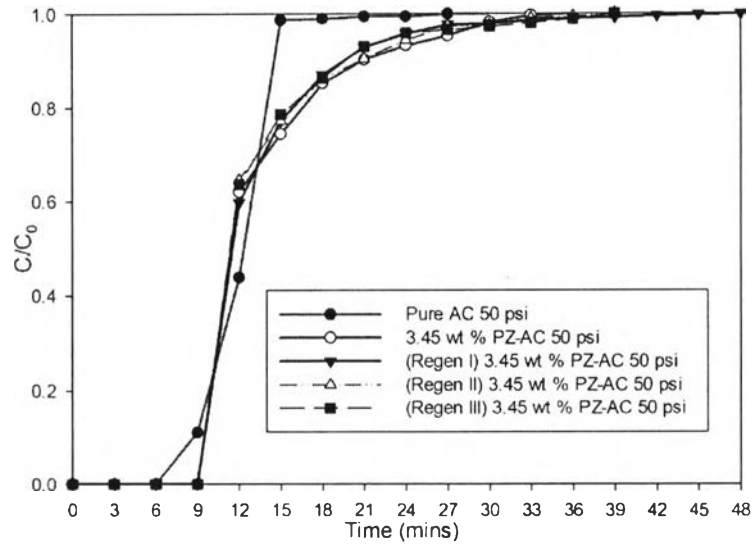

Figure 4.14 Breakthrough curves of PZ - AC adsorption at 50 psi, and regeneration cycle I, cycle II, cycle III at room temperature.

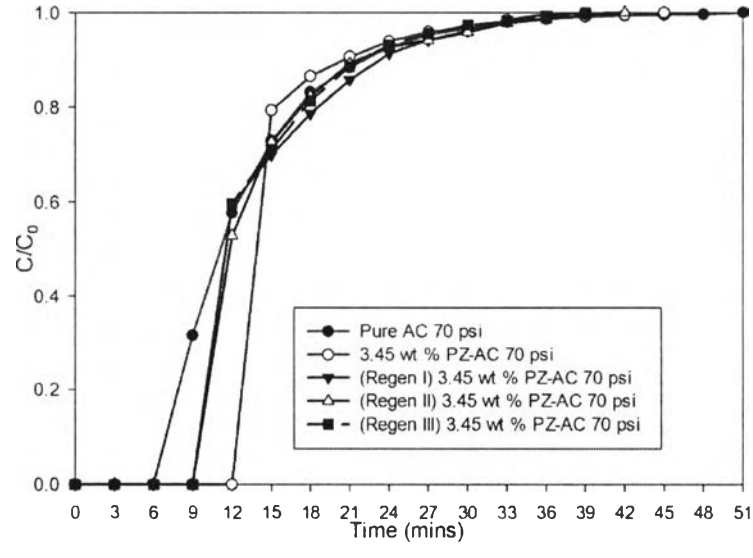

Figure 4.15 Breakthrough curves of PZ - AC adsorption at 70 psi, and regeneration cycle I, cycle II, cycle III at room temperature.

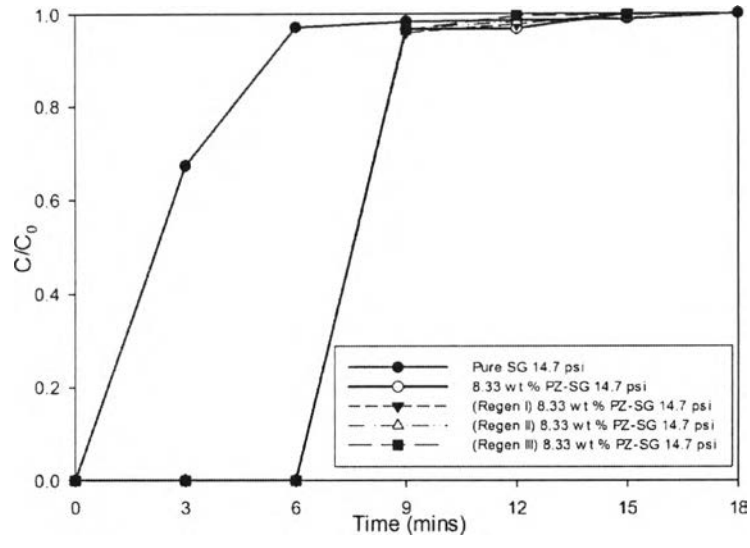

Figure 4.16 Breakthrough curves of PZ - SG adsorption at 14.7 psi, and regeneration cycle I, cycle II, cycle III at room temperature.

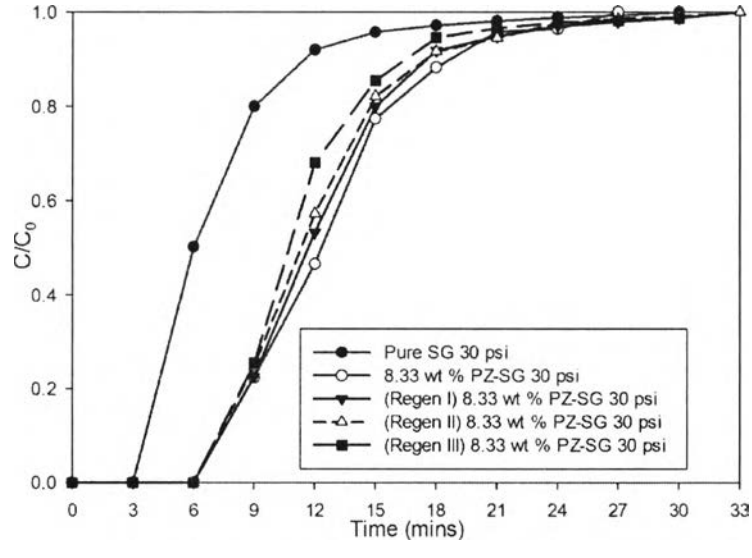

Figure 4.17 Breakthrough curves of PZ - SG adsorption at 30 psi, and regeneration cycle I, cycle II, cycle III at room temperature.

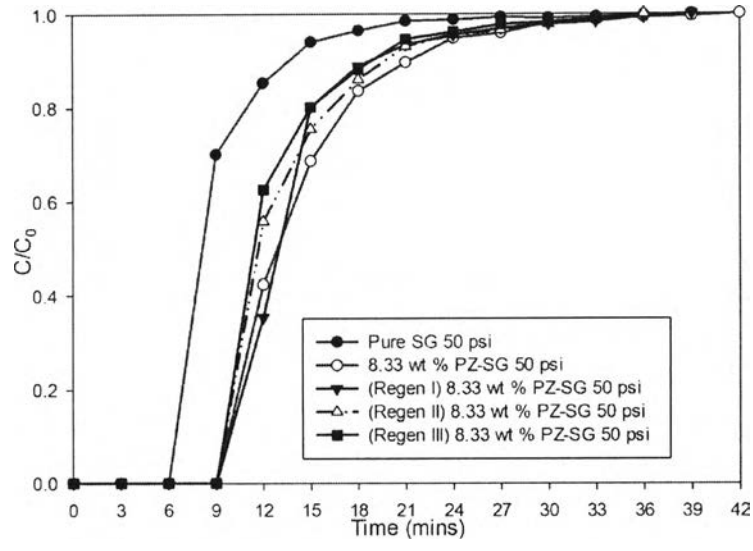

Figure 4.18 Breakthrough curves of PZ - SG adsorption at 50 psi, and regeneration cycle I, cycle II, cycle III at room temperature.

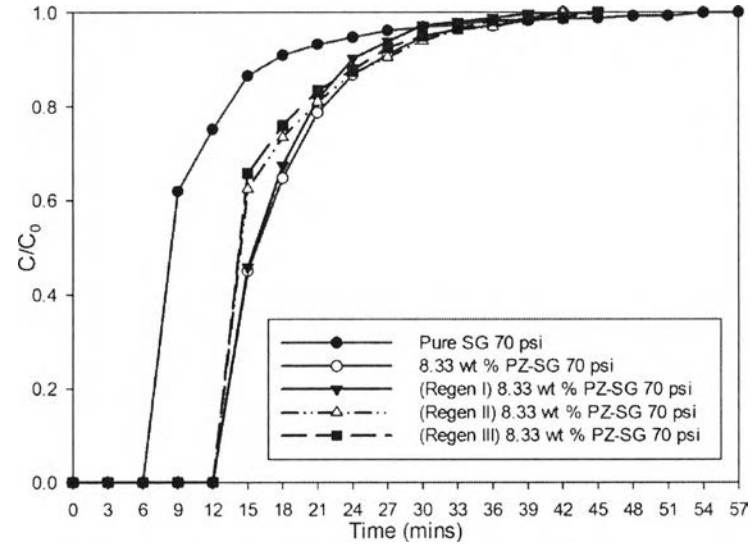

Figure 4.19 Breakthrough curves of PZ - SG adsorption at 70 psi, and regeneration cycle I, cycle II, cycle III at room temperature.

Table 4.5 The normalized CO_2 adsorption capacities of the 3.45 wt % piperazine-activated carbon ($\mu mol/m^2 \cdot g$) after regeneration

pressure (psi)	3.45 wt% PZ-AC	Regeneration (Cycle I)	Regeneration (Cycle II)	Regeneration (Cycle III)
14.7	0.8089	0.7264	0.6595	0.6061
30	2.6529	2.3558	2.3394	2.1918
50	4.9476	4.8850	4.8625	4.8392
70	7.9497	7.4111	7.3775	7.2429

Table 4.6 The normalized CO_2 adsorption capacities of the 8.33 wt % piperazine-silica gel ($\mu mol/m^2 \cdot g$) after regeneration

pressure (psi)	8.33 wt% PZ-SG	Regeneration (CycleI)	Regeneration (CycleII)	Regeneration (CycleIII)
14.7	1.4571	1.4560	1.4541	1.4433
30	4.9041	4.7965	4.6864	4.4621
50	9.2684	8.9839	8.7192	8.3842
70	16.1563	15.6284	15.4176	15.2864

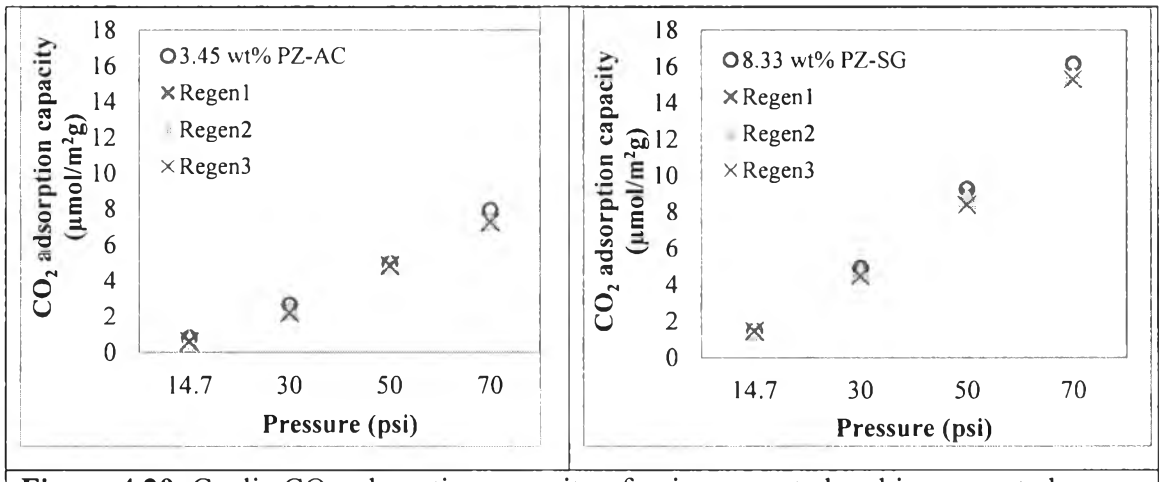

Figure 4.20 Cyclic CO_2 adsorption capacity of unimpregnated and impregnated adsorbents ($\mu mol/m^2 \cdot g$).

In the adsorbent regeneration, the adsorption was firstly performed after that the regeneration was achieved by purging with 113 mL/min pure nitrogen at atmospheric pressure and room temperature. When the chromatogram showed no sign of CO_2 response, the CO_2 adsorption was repeated using the first used adsorbent. The results show the decrease in CO_2 adsorption capacity after three consecutive cycles. From Table 4.5 and Table 4.6, the CO_2 adsorption capacity of the first run of impregnated adsorbent was higher than every regeneration cycles and it was seen that the more regeneration cycles used, the more efficiency dropped. The average efficiency of regeneration is 92.64 ±4.48, 90.20 ±7.10, and 86.61 ± 9.97% for 3.45 wt % PZ-AC and 97.85 ±1.46, 96.22 ±2.48, and 93.78 ±3.97 % for 8.33 wt % PZ-SG. This also indicated that the number of cycles increase, the efficiency of adsorbent was reduced. Figure 4.20 shows that the regeneration efficiency was not completely recovered due to the fact that some of the carbon dioxide molecules could still be adsorbed on the pore. The efficiency of regeneration of the impregnated AC and impregnated SG was more than 85 % and 90 %, respectively. Comparing with the impregnated SG, the impregnated AC show a higher drop in the CO_2 adsorption capacity with increasing cycles of regeneration. The comparison between the mesopore of SG and the micro- and mesopore of AC could show that the micropore of AC could be one of the main effects for CO_2 regeneration capacity which have the small pore for the interaction between the CO_2 molecules and the pore walls. Then, the CO_2 molecules could still be existed on the micropore of the AC which could effect to the higher drop in the efficiency of regeneration. In addition, Wang *et al.* (2012) suggesting that impregnated SG has more excellent regeneration stability because the carbon dioxide molecules could depart from the surface and pore of the mesoporous SG more easily than the micropore of AC.